Dynamic analysis of small droplets at constant pressure and analytical model for drip systems and very low pressure drop-on-demand applications

Thierry Thami, Christian Fretigny, Emilie Verneuil

▶ **To cite this version:**

Thierry Thami, Christian Fretigny, Emilie Verneuil. Dynamic analysis of small droplets at constant pressure and analytical model for drip systems and very low pressure drop-on-demand applications. Flow Measurement and Instrumentation, 2023, 91, pp.102369. 10.1016/j.flowmeasinst.2023.102369 . hal-04080114

HAL Id: hal-04080114
https://hal.umontpellier.fr/hal-04080114v1

Submitted on 24 Apr 2023

HAL is a multi-disciplinary open access archive for the deposit and dissemination of scientific research documents, whether they are published or not. The documents may come from teaching and research institutions in France or abroad, or from public or private research centers.

L'archive ouverte pluridisciplinaire **HAL**, est destinée au dépôt et à la diffusion de documents scientifiques de niveau recherche, publiés ou non, émanant des établissements d'enseignement et de recherche français ou étrangers, des laboratoires publics ou privés.

Journal Pre-proof

Dynamic analysis of small droplets at constant pressure and analytical model for drip systems and very low pressure drop-on-demand applications

Thierry Thami, Christian Fretigny, Emilie Verneuil

PII: S0955-5986(23)00065-1

DOI: https://doi.org/10.1016/j.flowmeasinst.2023.102369

Reference: JFMI 102369

To appear in: *Flow Measurement and Instrumentation*

Received Date: 12 December 2022

Revised Date: 31 March 2023

Accepted Date: 4 April 2023

Please cite this article as: T. Thami, C. Fretigny, E. Verneuil, Dynamic analysis of small droplets at constant pressure and analytical model for drip systems and very low pressure drop-on-demand applications, *Flow Measurement and Instrumentation* (2023), doi: https://doi.org/10.1016/j.flowmeasinst.2023.102369.

Journal Pre-proof

Dynamic analysis of small droplets at constant pressure and analytical model for drip systems and very low pressure drop-on-demand applications

Thierry Thami[a,*], Christian Fretigny[b], Emilie Verneuil[b,**]

(a) Institut Européen des Membranes, IEM, Université Montpellier, ENSCM, CNRS UMR5635, Place Eugène Bataillon, 34095 Montpellier Cedex 5, France

(b) Sciences et Ingénierie de la Matière Molle, UMR7615, ESPCI, CNRS, PSL Research University, Sorbonne Université 10 rue Vauquelin, 75231 Paris cedex 05, France

Correspondence to: T. Thami (thierry.thami@umontpellier.fr)

Shared correspondence to: E. Verneuil (emilie.verneuil@espci.fr)

Journal Pre-proof

ABSTRACT. We study the evolution of the growing volume of a droplet formed out of a capillary tube driven at a constant applied pressure by optical volume detection. A particular application aims at modeling the dynamic of the drop in the case of the injection of drugs in the middle-ear cavity using a small target drug delivery system. Various dispense tips such as a steel needle or silicone catheters and different *t*-BuOH aqueous solutions were used. A physical model based on the simplified Laplace–Young equation for a spherical droplet was developed to interpret the experimental results and model the observed deviation of the mean flow rate from the Poiseuille law when the drop radius is smaller than the capillary length. We emphasize the large influence of the surface tension which introduces a highly nonlinear effect at low applied pressure just above the capillary threshold pressure. The model fits well the evolution of the growing volume at various applied pressure up to a maximum diameter corresponding to the drop size close to the capillary length of the fluid, $l_c = \sqrt{\gamma/\rho g}$, based on the liquid density ρ, gravity g and surface tension γ. We demonstrate that the model can also be applied to non spherical pendant droplets providing the apex elongation over the drop height of a spherical cap of the same volume is kept in a 30% range.

KEYWORDS. Drip, Flow rate model, Capillary tube, Pendant drop, Drug delivery, Surface tension.

Journal Pre-proof

Journal Pre-proof

1. Introduction

The growth of liquid drops in air from the tip of a capillary tube has received considerable attention over the last past century [1–5]. In recent years, interest has raised for targeted drug delivery devices to improve the efficiency of therapeutic treatments by injecting the drug directly on the targeted tissues thereby overcoming physical barriers. The injection of drugs in the human body is a challenge relevant to biomedical application such as the treatment of inner ear disorders (or diseases) by local application of drugs [6–9]. We investigated the formation of droplets in air to provide a reliable dosing method for a delivery system implantable in the middle ear to deliver medications by filling a small niche at the entrance of the inner ear [10]. The safe and standardized surgical procedure for implantation and fixation of catheter consists in anchoring the catheter to bone [11] in the middle ear near the round window membrane (RWM) used as a main route for the transfer of potential substances to the inner ear [6,7,12]. The drops are deposited precisely within the RWM niche. The drugs are then selectively absorbed by the tissue and gently delivered to the perilymph of the inner ear. The key parameters for designing such a catheter tip for a long term implantation are the rheology of the drug formulation, the physical shape and the physicochemical surface properties of the tip [13] and the mechanism of drop growing.

In this study we aim to control the volume and the flow rate of drops containing drug solution in the air cavity of the middle ear. One challenge is the accurate placement of a drop containing the medication in the middle-ear cavity with the catheter tips at a distance of the order of 1 mm of the niche of the RWM in order to minimize the influence of gravity. Then, the growth could be stopped for a critical drop height less than 1 mm by contacting the RWM tissue. The drop would finally be absorbed by the tissue at the desired drug concentration. The

contact effect and following absorption mechanism is not considered here. The paper concentrates on the growing mechanism of the drop.

Regarding the miniaturization of pump devices, it is important to measure flow characteristics at the length scale of the implanted catheter according to the specification of pumps of small size such as MEMS pumps [14,15]. Two main characteristics of the fluidic circuit are to be characterized in relation with the design of the pumps, the threshold capillary pressure and its hydraulic resistance. We have investigated *in vitro* experiments of forming a droplet with dedicated catheters. A prototype of droplet delivery for R&D investigations has been designed (Fig. 1) to work at a constant pressure based on a gravity-driven liquid reservoir. The setup allowed us characterizing the evolution of the drop volume with time and the mean flow rate as a function of the applied pressure in dripping mode by using optical volume detection.

The experimental flow analysis developed method is relevant to accurately characterize the catheter system prior to using it *in vivo*. Several experiments of liquid dropping at controlled pressures have been designed to make it possible to measure both the hydraulic conductance and the flow rate behavior of typical implantable catheters. The measured characteristics of the capillary system can then be used to predict the fluidic behavior of any pump systems under a constant pressure or at a constant flow rate, though the characteristics of the drop detachment threshold may differ. Nevertheless, the miniaturization of implantable pumps for application in the middle ear remains a challenge.

As liquid is driven out of a capillary tube, a drop forms and grows. The growth stage can be divided into two phases depending on whether gravity can be neglected or not. The capillary length $l_c = \sqrt{\gamma/\rho g}$ can be compared to the drop height h in order to estimate the relative importance of the capillary pressure to the hydrostatic pressure drop over the drop height h.

At early stages h is smaller than l_c and the drop is quasi-spherical. As the drop grows, its shape elongates ($h \sim l_c$) until the drop falls.

Various physical models of the drop growing process have been previously published [1–5,16–28] regarding the case of the measurement of dynamic surface tension [29–31] or the case of constant volumetric flow rate or for passive pumping [32,33], in which the applied pressure is not constant. Indeed, in many cases, the pumping methods are well described by analytical models of expanding liquid drops where a constant flow rate is adjusted for example, by displacing at constant speed the piston of a high-precision syringe [1,18–20,23,26,29–31]. Thus it has been often proposed to treat the growing of droplets at constant flow rate in most applications. We present here for the first time an analytical model for droplet delivery apparatus in which, by contrast with previous models, the applied pressure is constant. The proposed model is based on the simplified Young-Laplace equation [5,29,30] for drop height h smaller than the capillary length l_c ($h \lesssim l_c$). The model incorporates design parameters such as surface tension, fluid viscosity and density, inner and outer radii of blunt tip (flat face tip) capillary tube permitting efficient use of our testing method by changing the geometry of the tip and the surface tension of the fluid. Drop on demand technology [34] is widely used and we offer that the proposed analytical model could easily be introduced in monitoring and production process control tools. This model has mainly been evaluated for drop size below the capillary length produced at pressure just above the capillary threshold pressure.

In this paper, the physical model was validated by comparing with the experimental observations of growing of drops from their initiation until they break up due to gravity. Surprisingly, the analysis domain can also be extended to elongated drops with a good correspondance.

2. Material and methods

Four liquids were used as test fluids with surface tensions γ ranging from 72 to 24 mN/m: deionized (Millipore) water and aqueous solutions of *t*-BuOH of mole fractions (x) = 0.1, 1.7 and 10% (mol%), (x) = [*t*-BuOH]/ ([*t*-BuOH] + [H_2O]) where [*t*-BuOH] and [H_2O] stand for the concentrations of *t*-BuOH and H_2O, respectively. The aqueous *t*-BuOH mixtures were prepared by weighting from 2-methyl-2-propanol (*tert*-butyl alcohol) of 99.7% purity (Aldrich) as received. The surface tension values at 22 °C (Accuracy 0.5%) were measured by the Wilhelmy method, using a standard precision 3S tensiometer supplied by GBX (Romans, France), and summarized in Table 1. They were found in agreement with reported data [35,36]. The density (ρ) and viscosity (η) of liquids used for numerical calculations are extrapolated from reported data [37,38] (Table 1).

Liquid mol%	Surface Tension γ^a mN/m	Density ρ^b kg/L	Dynamic Viscosity η^b mPa.s
H_2O	72.2	0.9978	0.955
t-BuOH 0.17%	60.1	0.9958	0.9192
t-BuOH 1.7%	40.1	0.9866	1.2475
t-BuOH 10%	23.6	0.9421	3.243

[a]Measured at 22 °C. [b]Extrapolated at 22 °C for water [37] and at 25 °C for water/*t*-BuOH mixtures data from ref. [38].

Table 1. Physical data for water and the water/*t*-BuOH system.

The experimental setup was designed to visually analyze the evolution of the volume of drops emerging from a capillary tip in air in a drop by drop mode as seen in Fig. 1a. This

figure includes a schematic of the system used to extract the drop volume from image analysis. All experiments were performed in normal ambient air at 23 ± 1 °C. The system was secured against unwanted gas bubbles in order to ensure accurate pressure measurement.

Silicone and stainless steel capillaries were used to analyze the influence of the wettability of the flat tip faces. Various tip sizes were also compared with outer diameters $2R_e$ ranging from 0.7 to 1.3 mm and inner diameter $2R_i$ ranging from 0.4 to 0.8 mm. Silicone tubes are referenced sil1.3 ($2R_e$ = 1.348 ; $2R_i$ = 0.846) and sil1.2 ($2R_e$ = 1.260 ; $2R_i$ = 0.630). Steel needles are referenced steel0.7 ($2R_e$ = 0.720 ; $2R_i$ = 0.414) and steel0.8 ($2R_e$ = 0.820 ; $2R_i$ = 0.552). Silicone tube lengths were carefully measured close to the 0.1 m specified for use with middle ear implantable systems. Steel0.7 tip is blunt end precision needle supplied by Hamilton of length 0.051 m. The tips of silicone tubes were cut flat and perpendicular to the axis of the tube and then cleaned with isopropyl alcohol and rinsed with water. The external radii R_e and inner radii R_i of the tips were measured using a microscope. The length of the silicone tubes L was systematically measured and L ranges between 0.050 and 0.200 m.

The drop growing process was captured using the video recording system of a GBX Digidrop (Contact Angle Meter) which provided a dimmable back-light and a standard CCD video camera system (Pixelink) of resolution 752 × 480 operating at a normal 40 ms frame rate. The GBX Visiodrop image analysis software set to axisymmetric drop shape analysis [39] was used to measure the drop growing volume $v(t)$ versus time.

To drive the different liquids through the capillary tubes, we used a gravitational-based reservoir system (Fig. 1a) so that the hydrostatic pressure $\Delta P = \rho g \Delta H$ generated by a column of liquid of height ΔH can be approximated as a constant pressure during the delivery of a few drops from a given liquid level. We estimated that the liquid level decrease is less than 20×10^{-3} m per drop for a typical falling drop volume of 15 µL when the reservoir diameter is as large

as 29×10^{-3} m. The capillaries were mounted on a holder in order to maintain the tip vertically. The tip position was precisely defined using a micrometer gauge. In order to vary the applied pressure, the height of the reservoir was moved up or down with a PC-controlled stepper motor dedicated for use with syringes and by precisely measuring ΔH that separates the meniscus of liquid in the reservoir from the flat cut of the capillary tip. Measuring the height with an estimated accuracy of $\pm0.25\times10^{-3}$ m led us control the applied pressure within the ±2.5 Pa range.

For all tested liquids and tips, the drop growth followed the same typical image sequence as shown in Fig 1b. During a first short period, the fluid moves out and wets the overall surface of the tip. In its initial state, the drop pins to the outer edge of capillary tip of radius R_e. Then a periodic discontinuous flow is reached with the drops growing and falling due to gravity. The neck formation (Fig. 1b) and detachment stage (not shown) were observed during a transient period of a few dozen of millisecond, while the growth phase ranges between 1 and 10 s, depending on the experimental conditions.

Journal Pre-proof

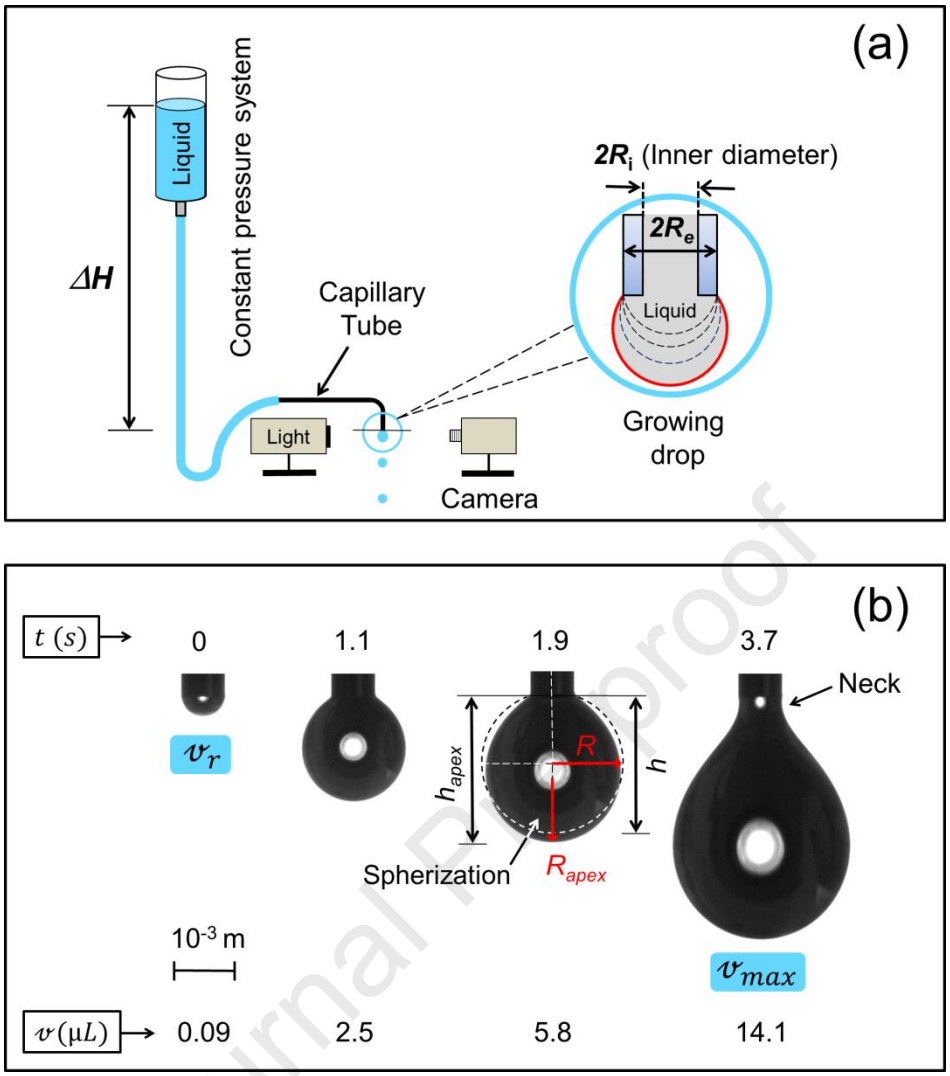

Fig. 1. (a) Dripping setup: the reservoir sets the pressure which is adjusted by its vertical position ΔH. Images of the drop are captured at the tip of the capillary tube. A close-up of the capillary tip is shown in inset. The drop volume $v(t)$ is extracted from the contour shape of the axisymmetric pendant drop. (b) A typical increasing size is shown according to time. The typical image sequence during drop growth was obtained using a steel0.7 tip. v_r is the initial volume of the growing drop which is the residual volume after previous drop break-up and v_{max} is the maximum volume before detachment. A spherization of the drop shape is shown where R and h denote respectively the radius and the height of equivalent spherical cap (dotted line) having identical volume of the drop. R_{apex} and h_{apex} are respectively the radius and the height measured at the apex of the drop elongated by gravity. R and h were calculated

from the analytical model of drop volume $v(t)$ using Eqs. (4–7,12). R_{apex} and h_{apex} were measured from calibrated volume image at time *t* using ImageJ software.

We define v_{max} as the maximum volume reached before the drop detaches from the tip and v_r as the residual volume after the drop breakup as shown in Fig 1b. We observed that the production of the drops corresponds to a steady state characterized by a repeatable maximum volume for each solution/tip combination used among different concentrations and tip outer diameters (Fig. 2). The residual drop is always hemispherical and pinned to the outer edge of the tip.

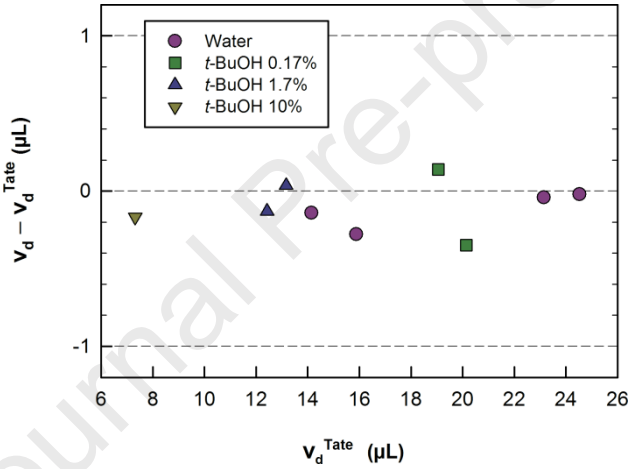

Fig. 2. Average ($v_d - v_d^{Tate}$) volume difference of the detached drops v_d as a function of the volume v_d^{Tate} determined by the corrected Tate's law. See text for more details. The outer diameters ($2R_e$) of the different tips used for the solutions were 0.720, 0.820, 1.260 and 1.348 mm (water), 1.260 and 1.348 mm (*t*-BuOH 0.17% and 1.7%) and 1.260 mm (*t*-BuOH 10%).

Fig. 2 shows the volume difference variations of the detached drops $v_d = v_{max} - v_r$ as a function of the corrected Tate volume [40,41]: $v_d = 2\pi f \gamma R_e/\rho g$ where γ is the surface tension, ρ is the density of the liquid, f is an empirical correction shape factor first experimentally determined by Harkins and Brown [24] and g = 9.81 m/s² is the gravitational constant. The values of f were calculated for all liquid/tube pairs tested in function of the

aspect ratio of the different tips, $x = R_e/{v_d}^{1/3}$ where v_d is the volume of detached drop, from a polynomial fit of the data [40,41] as $f = 0.7688x^2 - 1.0496x + 0.98707$. The error of v_d Tate's volume calculations is relatively minor compared to v_d measurements. The volume v_d was measured for different tube/solution pairs at a flow rate of approximately 5 µL/s so that evaporation effect of droplets present in alcohol-water mixtures is minimized because the corresponding drip periods of about 1 s were short. The good agreement with the Tate's law (Fig. 2) shows that the volume change due to the evaporation of the drop in the dripping mode is negligible. However, the main differences in Fig. 2 may also be due to other factors such as tip wettability. It is estimated that, based on Fig. 2, the accuracy of v_d measurements was between 0.3 and 2%.

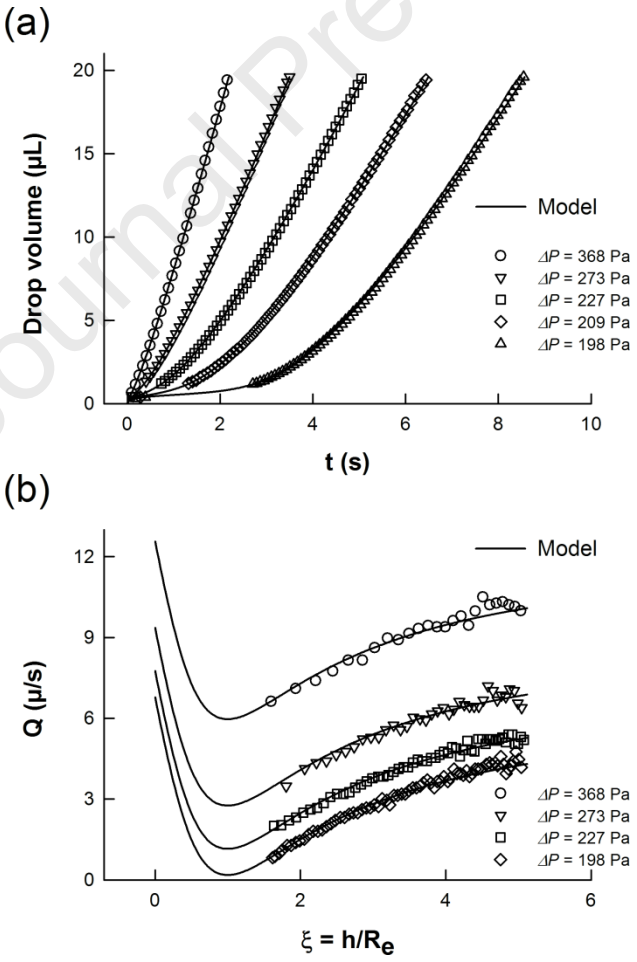

Journal Pre-proof

Fig. 3. (a) Instantaneous drop volume $v(t)$ from a capillary tip as a function of the time at varied imposed pressure (ΔP) from the lower v_r to the upper v_{max} limit volumes of the drip. The experimental curves are adjusted to the model in black solid lines using the liquid surface tension parameter of 60.8 mN/m determined by curve-fitting of the whole $v(t)$ curves (see Section 4.2). For clarity, not all data collected were shown on the plateau. (b) Flow rate $Q(t)$ calculated from the time derivative of the drop volume data, plotted at varied imposed pressure (ΔP) as a function of the normalized height $\xi = h/R_e$. Black solid lines are the model curves $Q(\xi)$ calculated with the fit parameters found by curve-fitting the volume curves. The dimension of the capillary silicon tip (sil1.2) was R_e = 0.630×10^{-3} m (v_h = 0.52 µL). The measured hydraulic resistance was determined by fitting line plots of flow rate versus pressure and averaging (see Section 4.1): R_h = 29.2 Pa.s/µL with an aqueous solution of *t*-BuOH 0.17% (mol%) used in the drip.

For each couple liquid-capillary tip, a series of experiments were performed where the pressure was varied in the 100 to 400 Pa range. The kinetics of the growth volume was measured over time as shown in Fig. 3. In each case, a pressure threshold is observed below which no dripping occurs. A theoretical model is developed below to account for these observations.

3. Description of the model

In the following, we suppose that the drop shapes remain approximately spherical and can thus be described by a radius of curvature $R(t)$ which increases over time. This assumption is valid at the early stages of the growth as confirmed by the observations (Fig. 1b). It is theoretically expected to hold as long as the drop height h compares with the capillary length l_c. It will be shown that its validity domain can be extended until the drop detachment.

The liquid surface tension γ induces a capillary pressure in the drop $P_{cap}(t) = 2\gamma/R(t)$ where *R(t)* is the radius of the drop. When this pressure is higher or equal to the applied pressure from the reservoir, no flow occurs. When it is lower, liquid flows. The flow rate is related to the pressure difference by the well-known model of Poiseuille in circular tubes of inner radius R_i:

$$\Delta P - P_{cap}(t) = R_h Q(t) \tag{1}$$

where R_h is the corresponding hydraulic resistance. In our experiment, the pairing of the capillary tube to the reservoir was designed so that the source of hydrodynamic pressure loss within the connections between the capillary and the reservoir systems are negligible yielding:

$$R_h = 8\,\eta L/\pi\, R_i^4 \tag{2}$$

where η is the viscosity of the fluid, L is the length of tube. We denote $\lambda = 2\gamma/(R_e \Delta P)$ the ratio of the residual drop capillary pressure to the applied external pressure. If $\lambda > 1$ the residual drop does not grow. In the dripping mode, the experimental pressure ratio was $0.4 \lesssim \lambda \lesssim 0.998$. Using Eq. (1), the flow rate Q that feeds the drop writes:

$$Q(t) = \frac{\Delta P}{R_h}\left(1 - \lambda \frac{R_e}{R_\lambda(t)}\right) \tag{3}$$

On the other hand, the volume of the drop $v(t)$ is given by: $v(t) = \frac{\pi}{2} h({R_e}^2 + \frac{h^2}{3})$ while h, R_e and R_λ are linked by the geometrical relation for spheres: ${R_\lambda}^2 = (h - R_\lambda)^2 + {R_e}^2$ where $R_\lambda(t)$ is the calculated radius of curvature of the drop and the subscript λ refers to the dimensionless pressure applied to the drop. This indicates in Eq. (3) that the drop radius will also change with the applied pressure (or the value of λ). Introducing the dimensionless parameters:

$$\xi = h/R_e \tag{4}$$

$$V = v/v_h \tag{5}$$

where $v_h = 2\pi R_e^3/3$ is the volume of the hemispherical cap of radius R_e, the normalized drop volume V and its radius of curvature R_λ write:

$$V = \frac{3}{4}\xi\left(1 + \frac{\xi^2}{3}\right) \tag{6}$$

$$\frac{R_\lambda}{R_e} = \frac{\xi^2+1}{2\xi} \tag{7}$$

Hence, the flow rate can be derived from Eq. (6) and (7):

$$Q = \frac{dv}{d\xi}\frac{d\xi}{dt} = \frac{3}{4}v_h(\xi^2+1)\frac{d\xi}{dt} \tag{8}$$

The flow rate given by Eq. (3) can also be recast using the dimensionless parameters. Introducing the characteristic growth time τ:

$$\tau = \frac{\pi}{2}\frac{R_h R_e^3}{\Delta P} \tag{9}$$

the two different equations for the flow rate Q in Eqs. (3) and (8) lead to the differential equation for the evolution of the normalized height of the drop $\xi(t)$:

$$\frac{(1+\xi^2)^2}{1-2\lambda\xi+\xi^2}d\xi = \frac{dt}{\tau} \tag{10}$$

This yields:

$$\mathrm{Q}(\xi) = \frac{\frac{3}{4}(1+\xi^2)^3}{1-2\lambda\xi+\xi^2}\frac{v_h}{\tau} \tag{11}$$

The characteristic time τ is the time at which the capillary term no longer impairs the drop growth as seen from Eq. (3). Solving the differential equation Eq. (10) leads to a parametric representation of the volume as a function of time: $V = V(\xi)$ is given by Eq. (6) and $t = \tau\varphi_\lambda(\xi)$ with:

$$\varphi_\lambda(\xi) = \frac{\xi^3}{3} + \lambda\xi^2 + (1+4\lambda^2)\xi + 4\lambda^3\ln(\xi^2 - 2\lambda\xi + 1)$$
$$+4\lambda^2\frac{1-2\lambda^2}{\sqrt{1-\lambda^2}}\left[\tan^{-1}\frac{\lambda-\xi}{\sqrt{1-\lambda^2}} - \tan^{-1}\frac{\lambda}{\sqrt{1-\lambda^2}}\right] \tag{12}$$

Solutions to this equation exist for $\lambda < 1$ only, as expected, because drop growth imposes the condition $d\xi/dt > 0$. We therefore define a pressure threshold $P_{th} = 2\gamma/R_e$: the applied pressure ΔP must be larger than P_{th} for the dripping to occur.

4. Discussion

4.1. Kinetics

The overall evolution curves of the instantaneous drop volume $v(t)$ are presented in Fig. 3a for a typical series of experiments at varied imposed pressure. In order to compare the experimental data to the model, it can be noticed that while the drop volume v is directly obtained from image analysis, its theoretical variations over time requires the resolution of the differential equation Eq. (10). The instantaneous flow rate $Q(t)$ was determined from a sufficiently fast recording of images by time derivation of the drop volume data extracted from the images and was plotted against the normalized height $\xi = h/R_e$. On the other hand, the flow rate Q is readily obtained from the model as a function of the reduced height from Eq. (11) while both Q and ξ are deduced from the data by time derivation of the volume and solving Eq. (6) respectively. As a result, both comparisons are presented in Fig. 3, namely $v(t)$ and $Q(\xi)$. Note that ξ is the height of the equivalent spherical cap having volume v as depicted in Fig. 1b. It may differ from the actual drop height if the drop is elongated by gravity as will be discussed later.

The comparison between experiments and theoretical model was done in two steps. First, for each tube, the hydraulic resistance R_h was measured from the flow rate curves $Q(\xi)$ at varied pressure ΔP by plotting $Q(\Delta P)$ at constant drop volumes to determine the slope as seen from Eq. (3) and in the inset graph of Fig. 4a. We then calibrated the hydraulic R_h resistance by averaging values determined at varied drop volume (Fig. 4b). The experimental time-volume curves were finally adjusted to the model curves by finely tuning the fitting-parameter λ_{fit} in

both Eqs. (6) and (12) and by adjusting an offset to the experimental time so that the drop volume extrapolates to zero at time t = 0. An example is shown in Fig. 3 for an experiment performed with an aqueous solution of *t*-BuOH 0.17%.

First, we find a good agreement between the model and experiments for both $Q(\xi)$ and $v(t)$ curves, even for elongated drops for which the spherical cap hypothesis no longer holds. We will discuss later the limits of this hypothesis. The experimental instantaneous flow rate curves *Q(t)* in Fig. 3b agree with the model when $\xi > 1$. The proposed model shows V-shaped $Q(\xi)$ curves (Fig. 3b) with minimum flow at $\xi = 1$ when the capillary forces become relatively large compared to gravity for a drop of radius close to the tip radius, see Eq. (3). When $\xi < 1$, the drop radius *R(t)* and *Q(t)* decrease until $R(t) = R_e$ due to the increase in Young-Laplace forces.

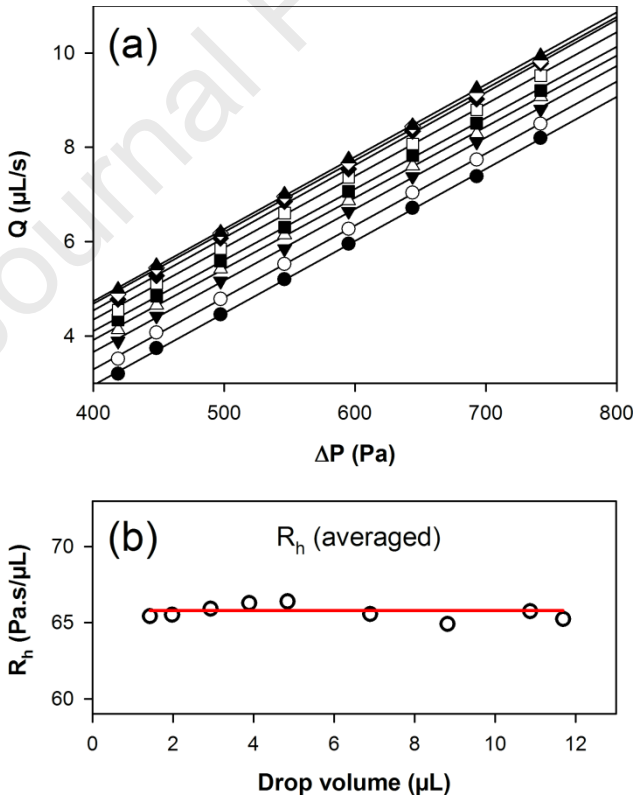

Fig. 4. Measurement of hydraulic resistance R_h using dripping for a single liquid/tube pair from the slopes of the instantaneous flow rate *Q(t)* versus pressure ΔP determined at constant

drop volume. (a) The whole linear plots Q(ΔP) at different drop volumes are shown. (b) Mean value of R_h = 65.8 Pa.s/µL (red line) by calculating the average of nine slope measurements at constant drop volume. The capillary tube dimensions (steel0.7) and properties of water used for the drip are given in Section 2.

Fig. 5 shows the variations of the hydraulic resistance difference as a function of the value expected from the Poiseuille model Eq. (2): $R_h = 8\,\eta L/\pi\, R_i^4$ for all pairs liquid/tube we tested. A relatively low resistance difference is observed for the steel/water capillary tube couple (Accuracy 6%) whereas the difference seems to increase with the value of R_h in the case of silicone material. Thus, the hydraulic resistance should be measured whenever possible to include it in the model. This is especially useful in cases where the inner radius of the capillary tube is not homogeneous or poorly accurate. We indeed found it was often the case for silicone capillaries.

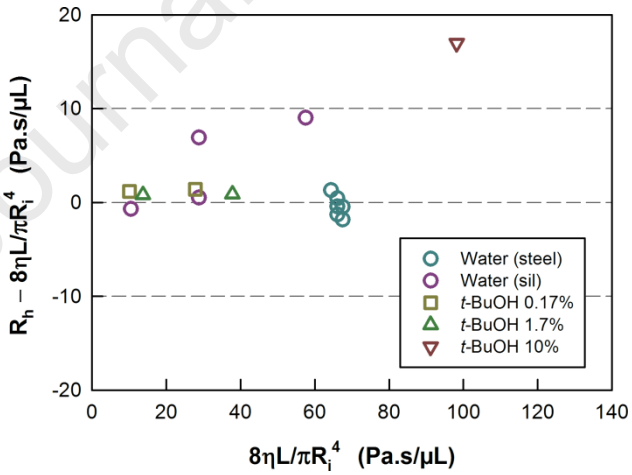

Fig. 5. Average hydraulic resistance difference ($R_h - 8\eta L/\pi R_i^4$) determined by dripping for different liquid/tube pairs as a function of the values expected from the Poiseuille model for circular tubes of inner radius R_i and length L (See dimensions in Section 2). The viscosity η of the different liquids used for the calculations are the same as those listed in Table 1.

4.2. Measurement of liquid surface tension

Next, the fitting parameter lambda can be used to measure the surface tension of the liquid through $\lambda = 2\gamma/(R_e\Delta P)$: as lambda is fitted to the whole $v(t)$ curve, it yields a measurement of surface tension of great accuracy. In Fig. 6, lambda is plotted as a function of $2/(R_e\Delta P)$ for a single liquid/tube pair and the slope gives a measure of the liquid surface tension as indicated by a good correlation coefficient (R = 1.0000) with an accuracy of 0.3% for water, as side result of the work. Fig. 7 shows the results obtained for all liquid tested as a function of the surface tension determined by the Wilhelmy method (Table 1). The latter method was used as a reference standard with an accuracy of 0.5%. We find a very good agreement between the two methods for liquid/tube pairs with pure water and a 0.17% *t*-BuOH solution. By testing the reproducibility of measurement results with the water/steel0.7 couple (Fig. 7), the accuracy of the proposed drop method was estimated at 1.5%. This shows that the dripping from a capillary tube at imposed pressure can be used as a simple set up to measure liquids surface tension. Only a camera, a reservoir and a capillary tip are necessary. Nevertheless, in the case of *t*-BuOH solutions of increasing concentrations (1.7% to 10%), the surface tensions measured by the drop method are overestimated because of the evaporation of alcohol-water mixtures.

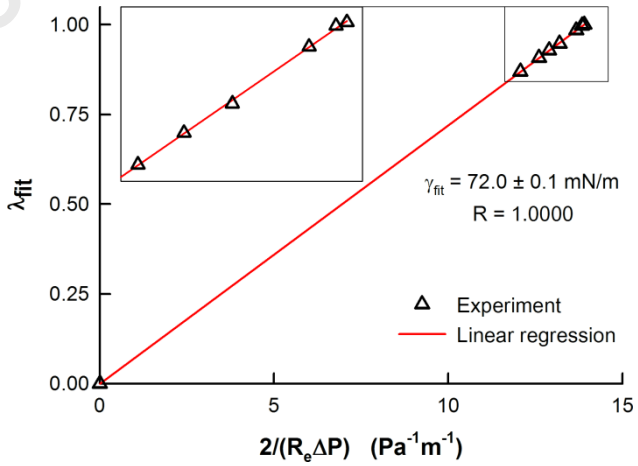

Fig. 6. Measurement of liquid surface tension γ using dripping of a single liquid/tube pair at varied pressure ($\lambda \geq 0.85$), by plotting λ_{fit} used to adjust the whole $v(t)$ curves as a function

of $2/(R_e\Delta P)$. A greater emphasis on linear fitting of the data is shown (see inset). The external radius of capillary tube (steel0.7) and hydraulic resistance used for the fitting process were: R_e = 0.36×10^{-3} m and R_h = 65.8 Pa.s/µL (Fig. 4b) with water.

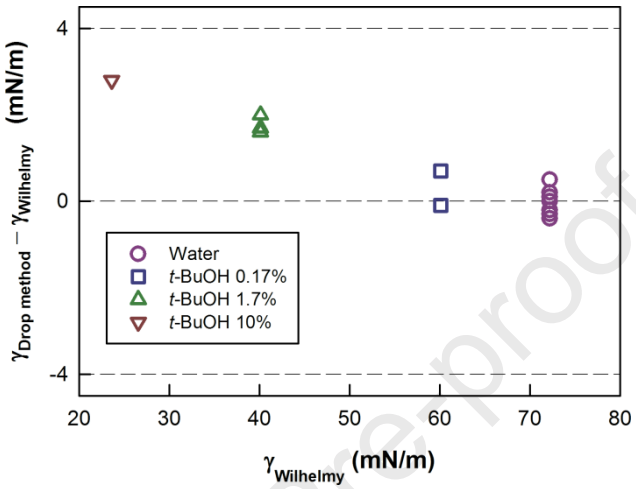

Fig. 7. Liquid surface tension difference $\gamma_{\text{Drop method}} - \gamma_{\text{Wilhelmy}}$ measured at 23 ± 1 °C determined by the drop method for all liquids tested by dripping by using different liquid/tube pairs in function of the surface tension γ_{Wilhelmy} determined by the Wilhelmy method.

4.3. Formation of the plateau

We emphasize in Fig. 8 the large influence of the surface tension which introduces a highly nonlinear effect at low applied pressure just above the capillary threshold pressure P_{th}. A plateau is observed at the hemispherical stage $R \sim R_e$ of the drop growing when the pressure is close to the internal capillary drop pressure term $\lambda \sim 1$ as seen in Eq. (3). From the pre-hemispherical period of the drop ($R > R_e$), the delay time to reach the hemispherical stage at $R = R_e$ increases and diverges as the applied pressure approaches P_{th} according to Eq. (12) for $\xi = 1$ and $\lambda \sim 1$. Experimentally, a delay time of few seconds could be measured (Fig. 8) before the expansion of the droplet occurs in the final stage in very good agreement with the model prediction. The theoretical curve starts with a jump at $t = 0$ with flow rate $Q(t = 0) =$

$\Delta P/R_h$ before reaching the plateau following a Poiseuille type law because the capillary pressure ($2\gamma/R \sim 0$) is negligible at the beginning. The time to jump at $\frac{3}{4}v_h$ is equal to ~ 6τ where τ is the characteristic growing time determined from Eq. (9). Then, the flow rate decreases drastically on the plateau because the delay time diverges (see above). As a drop grows from a capillary for an applied pressure greater than the threshold pressure ($\lambda < 1$), the capillary pressure in the drop $P_{cap}(t) = 2\gamma/R(t)$ increases until to a maximum which is obtained when the drop has the shape of a perfect hemispherical cap, with a diameter equal to the tip size of the dispensing capillary ($2R(t) = 2R_e$). As the drop further grows, the capillary pressure decreases because its radius increases. An inflexion of the flow rate is thus observed for $R(t) = R_e$. When the pressure increases, the plateau disappears but the inflexion on the flow rate is clearly shown on Fig. 8 (curve at higher pressure) in very good agreement with the model simulation.

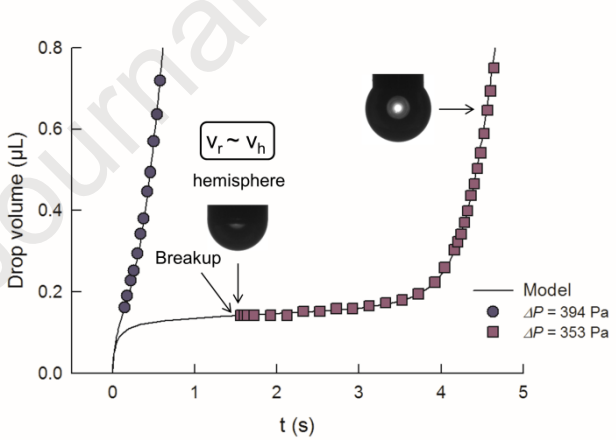

Fig. 8. Zoom of drop volume $v(t)$ curves by dripping showing formation of a plateau at imposed pressure *ΔP* close to the calculated threshold pressure P_{th} = 352 Pa and fitted model curves for the stainless steel (steel0.8) capillary tube/water pair. Two cases are shown at high pressure of 394 Pa and at 353 Pa for which the plateau is observed in good agreement with the model. The volume of the residual drop v_r formed an instant after the breakup is assumed hemispherical in form.

4.4. Limit of validity and accuracy of the model

A good agreement between experiments and analytical model could be reached up to an upper limit volume given approximately by the capillary length. Next we analyze the range of acceptable elongation of the drops for which the model, which assume drops are spherical caps, holds. The shape of the drop were quantified through the Bond number $Bo = \rho g R_{apex}^2/\gamma$ which measures the importance of gravitational forces relative to surface tension forces, while the size of the drop is determined by R_{apex} or h_{apex} (Fig. 1b). Chesters [16] showed that the profile of small pendant drop symmetrical about a vertical axis deviates from the spherical case (zero gravity) from the apex by increasing the shape factor (*Bo*) due to the effect of gravity. An analytical solution of the profil of the lower part of a pendant drop was found by perturbation methods with a small deviation of the profile from the circle. The profile, the height and the maximum volume of a pendant drop were then calculated for low *Bo* values less than about 0.1 for which the model of Chesters holds.

The profile of small drop is spherical at the apex [16] and R_{apex} can be easily measured using ImageJ software. Hence, the drop elongation can be expressed in dimensionless variable by $y = h_{apex}/R_{apex}$. Fig. 9 shows examples of evolution of *y* versus *Bo* during the growing process for three liquid/tube pairs at constant pressure for which the model applies until detachment of the drop occurs. The first stage of the curves starts when meniscus first appeared out of the capillary while R_{apex} dramatically decreases. During the second stage, *y* increases smoothly due to the shape variation of the drop from spherical to elongated profile. The final stage corresponds to the instant just before the neck formation. It is observed experimentally that the model applies well to all catheters with a tip radius to capillary length ratio R_e/l_c between 0.13 to 0.39 with $l_c = \sqrt{\gamma/\rho g}$. The spherical cap model fits the drop volume of elongated drop even for high bond numbers of 0.35 giving drop elongation *y* up to ~ 3.25 at the maximum volume that is reached before part of the drop breaks off. The

maximum volume, at which the model predictions are consistent with the experimental volume before detachment, corresponds to radius at the apex close to the capillary length of the fluid (Fig. 9). This shows that the model can be applied to many capillary tubes tips typically used in the field of biomedical application. We find that our model fits to the volume curves with good agreement and offers an accuracy of 3% estimated for 3 to 4 pressure values (ex. Fig. 3 with R_e/l_c = 0.25) during the whole history of the drop, for an elongation of drop compared to the height of the equivalent spherical drop of the order of 30%. For the case of *t*-BuOH 10%/sil1.2 tube pair (R_e/l_c = 0.39), the accuracy has been reduced to about 5% for an acceptable fit of the curves because the drop volume is small (see also Section 4.5).

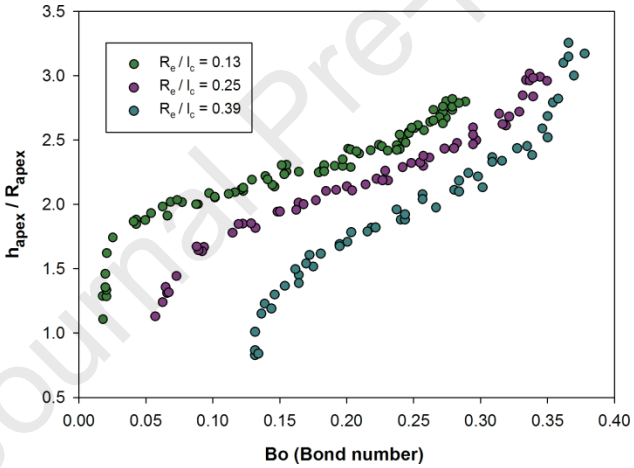

Fig. 9. Analysis of the elongation of a pendant drop h_{apex} /R_{apex} versus the shape factor *Bo* (Bond number) during the drop growing at constant pressure (4 to 5 values of pressure), for three liquid/tube pairs, water/steel0.7, *t*-BuOH 0.17%/sil1.2 and *t*-BuOH 10%/sil1.2, by varying the R_e/l_c ratio from 0.13 to 0.39 for which the spherical cap model for a pendant drop attached to a tube holds until the maximum volume was reached.

4.5. Dripping flow rate at constant applied pressure

In this section, we evaluate the validity of the model for calculating the mean flow rate Q_{tot} of the drip delivery system at a controlled applied pressure ΔP for applications in order to predict the flow rate of drop delivery systems before use *in vivo*. One can calculate the experimental flow rate of the dripping flow define as:

$$\mathrm{Q}_{tot} = \frac{v_{max} - v_r}{t_{max}} = \frac{v_d}{t_{max}} \tag{13}$$

where t_{max} is the time interval between detachment and initial time. For pressure higher than the threshold pressure P_{th}, the periods of the drip between v_r and v_{max} are constant for about 3 consecutive drops delivered at constant ΔP with a difference less than 40 ms. As shown in Fig. 2, the detachment volume is well described by the modified Tate's law: $v_d = 2\pi f \gamma R_e/\rho g$ and the residual volume not detaching from the capillary is well described by a hemisphere of radius R_e, with volume v_h (See Fig. 8). Note that in cases when the residual volume may be smaller than that of the hemisphere, the time needed to grow up to the hemisphere v_h is small compare to the total drop growth time. Hence, the initial time can be taken equal to the time when the drop is a hemisphere, corresponding to $\xi = 1$ in our model.

The mean flow rate of the dripping system can therefore be estimated from the theoretical model using Eq. 12 applied to the drop that detaches, that is for $\xi = \xi_d$ where ξ_d verifies:

$$v_h + v_d = \frac{3}{4}\xi_d \left(1 + \frac{{\xi_d}^2}{3}\right) v_h \tag{14}$$

and

$$\mathrm{Q}_{tot}(\lambda) = \frac{2\pi f \gamma R_e/\rho g}{\tau(\varphi_\lambda(\xi_d) - \varphi_\lambda(1))} \tag{15}$$

The total flow rate was measured for various applied pressures ΔP (or equivalently λ) and the result is plotted in Fig. 10. The model (Solid lines) is based on numerical calculation with Eq. (15). The model fits the experimental flow rate Q_{tot} with good accuracy between 0.5% to 2% in the linear region at different pressures. The estimated model accuracy of 10% at the start of the plateau may be improved by more accurately measuring the hydrostatic pressure.

We can simplified the mean flow curve model in the linear part of the $Q_{tot}(\Delta P)$ curves for volume interval v_d by writing $Q_{tot}\ (v_d) = Q(v_m)$ as follows:

$$Q_{tot} \sim \frac{1}{R_h}\left(\Delta P - \frac{2\gamma}{R(\xi_m)}\right) \quad (16)$$

where v_m is a mean drop volume included in the v_d interval and $R(\xi_m)$ is determined from Eq. (7). This linear relationship can be seen as a Poiseuille type law with a threshold pressure so that the mean flow rate of the drip system is always lower than a closed tube owing to a constant threshold shift $(\Delta P - \frac{2\gamma}{R(\xi_m)})$ due to the capillary pressure term generated by the drip.

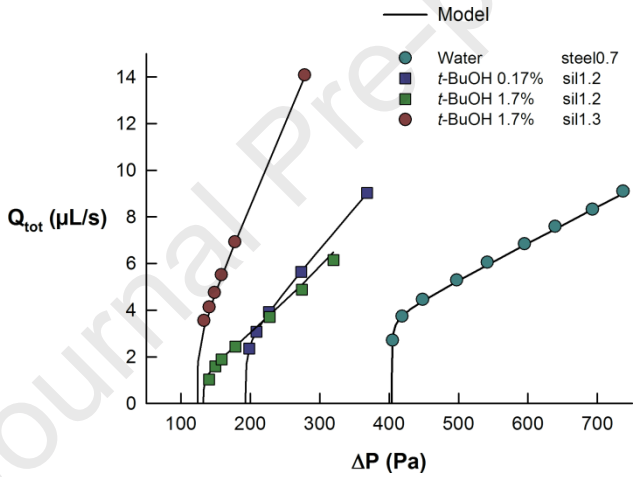

Fig. 10. Variation of mean flow rate Q_{tot} of the dripping system with pressure ΔP for different liquid/tube pairs. Simulated (black line) and experimentally measured (symbol) values are compared.

4. Conclusions

The simplified Young-Laplace equation was used to describe the growing drop process in the dripping mode. Various pairs of tubes and fluids such as water and *t*-BuOH mixtures were tested with the model by optical volume detection with a standard camera until part of the drop breaks off. The maximum volume v_{max} to which the model can be applied is highlighted with capillary tubes typically used in biomedical applications or for capillary tubes whose ratio between the radius of the tip and the capillary length R_e/l_c is between 0.13 to 0.39 with $l_c = \sqrt{\gamma/\rho g}$. The maximum volume corresponds to the elongation of the drop compared to the height of the equivalent spherical drop of order 30% and to the corresponding maximum Bond number of 0.37. We found that the model can even be applied satisfactory with 3% volume accuracy during the entire history of the drop with a large capillary silicone tube. The nonlinear evolution of the flow rate at constant applied pressure near the capillary threshold pressure is characterized by a plateau and a delay time which was measured in good agreement with model prediction.

We have developed a novel method to measure the surface tension of liquid by taking advantage of the evolution of the volume curves with time observed at controlled pressure near the threshold pressure. The accuracy of surface tension measurement by the drop method was estimated to be around 0.5% with water by fitting the entire $v(t)$ curve at different pressures for a single experiment and 1.5% after testing the reproducibility in air of a blunt end precision needle (Hamilton). The physical model was also developed in order to establish the evolution of the mean volumetric flow rate of the drop as a function of the applied pressure. As expected for drop sizes close to the capillary length, the model can predict the mean flow rate in perfect agreement with the experimental data and offers accuracy ranging from 0.5 to 2% in the linear part of curves following a Poiseuille type law. Accuracy was reduced to 10% in the plateau where pressure measurement accuracy was poor. To conclude, the analytical model facilitates the design of miniaturized drip delivery systems with water or

aqueous mixtures and permits the control of standard capillary systems prior to their usage *in vivo* conditions.

Acknowledgements

This work was supported in part by Sanofi and AVIESAN under project SAMI (Titled: Implantable System for Drug Delivery for the Treatment of Deafness and Tinnitus). We are grateful for Elisabeth Delevoye (Coordinator of SAMI project at CEA-Leti Grenoble) for helpful discussions, encouragements and very valuable comments and suggestions for the introduction of the manuscript. We thank CNRS for financial support.

References

[1] X. Zhang, Dynamics of Growth and Breakup of Viscous Pendant Drops into Air, J. Colloid Interface Sci. 212 (1999) 107–122. https://doi.org/10.1006/jcis.1998.6047.

[2] M.P. Brenner, X.D. Shi, S.R. Nagel, Iterated Instabilities during Droplet Fission, Phys. Rev. Lett. 73 (1994) 3391–3394. https://doi.org/10.1103/PhysRevLett.73.3391.

[3] B. Ambravaneswaran, S.D. Phillips, O.A. Basaran, Theoretical Analysis of a Dripping Faucet, Phys. Rev. Lett. 85 (2000) 5332–5335. https://doi.org/10.1103/PhysRevLett.85.5332.

[4] P.-G. de Gennes, F. Brochard-Wyart, D. Quéré, Gouttes, bulles, perles et ondes, Belin, Paris, 2005.

[5] M. Gentes, G. Rousseaux, P. Coullet, P.-G. De Gennes, Résolution de l'équation de Young–Laplace par une méthode géométrique utilisant la courbure, C. R. Phys. 6 (2005) 1027–1033. https://doi.org/10.1016/j.crhy.2005.11.009.

[6] A.N. Salt, S.K. Plontke, Principles of local drug delivery to the inner ear, Audiol. Neurootol. 14 (2009) 350–360. https://doi.org/10.1159/000241892.

[7] A.N. Salt, S.K.R. Plontke, Local inner-ear drug delivery and pharmacokinetics, Drug Discov. Today. 10 (2005) 1299–1306. https://doi.org/10.1016/S1359-6446(05)03574-9.

[8] M. Praetorius, A. Limberger, M. Muller, R. Lehner, B. Schick, H.P. Zenner, P. Plinkert, M. Knipper, A novel microperfusion system for the long-term local supply of drugs to the inner ear: Implantation and function in the rat model, Audiol. Neurootol. 6 (2001) 250–258. https://doi.org/10.1159/000046130.

[9] A.A. McCall, E.E.L. Swan, J.T. Borenstein, W.F. Sewell, S.G. Kujawa, M.J. McKenna, Drug delivery for treatment of inner ear disease: current state of knowledge, Ear Hear. 31 (2010) 156–165. https://doi.org/10.1097/AUD.0b013e3181c351f2.

[10] E. Delevoye, J.P. Nikolovski, T. Thami, F. Venail, S. Schmerber, Dispositif piézoélectrique de nano−dispense de fluides en spray ou en goutte−à−goutte : vers de nouvelles thérapies de l'oreille interne, 122ème Congrès de la Société Française d'Oto−Rhino−Laryngologie et de Chirurgie de la Face et du Cou, (2015).

[11] S.K. Plontke, R. Zimmermann, H.P. Zenner, H. Löwenheim, Technical note on microcatheter implantation for local inner ear drug delivery: surgical technique and

safety aspects., Otol. Neurotol. 27 (2006) 912–917. https://doi.org/10.1097/01.mao.0000235310.72442.4e.
[12] A.A. Mikulec, J.J. Hartsock, A.N. Salt, Permeability of the round window membrane is influenced by the composition of applied drug solutions and by common surgical procedures., Otol. Neurotol. 29 (2008) 1020–1026. https://doi.org/10.1097/mao.0b013e31818658ea.
[13] A.W. Adamson, A.P. Gast, Physical Chemistry of Surfaces, Wiley, New York, 1997.
[14] A. Nisar, N. Afzulpurkar, B. Mahaisavariya, A. Tuantranont, MEMS-based micropumps in drug delivery and biomedical applications, Sens. Actuators B Chem. 130 (2008) 917–942. https://doi.org/10.1016/j.snb.2007.10.064.
[15] N.-T. Nguyen, S.T. Wereley, Fundamentals and Applications of Microfluidics, Third Edition, Artech House, Boston-London, 2002.
[16] A.K. Chesters, An analytical solution for the profile and volume of a small drop or bubble symmetrical about a vertical axis, J. Fluid Mech. 81 (1977) 609–624. https://doi.org/10.1017/S0022112077002250.
[17] O.E. Yildirim, Q. Xu, O.A. Basaran, Analysis of the drop weight method, Phys. Fluids. 17 (2005) 062107. https://doi.org/10.1063/1.1938227.
[18] B. Ambravaneswaran, H.J. Subramani, S.D. Phillips, O.A. Basaran, Dripping-Jetting Transitions in a Dripping Faucet, Phys. Rev. Lett. 93 (2004) 034501. https://doi.org/10.1103/PhysRevLett.93.034501.
[19] B. Chang, G. Nave, S. Jung, Drop formation from a wettable nozzle, Commun. Nonlinear Sci. Numer. Simul. 17 (2012) 2045–2051. https://doi.org/10.1016/j.cnsns.2011.08.023.
[20] Z. Che, T.N. Wong, N.-T. Nguyen, Y.F. Yap, J.C. Chai, Numerical investigation of upstream pressure fluctuation during growth and breakup of pendant drops, Chem. Eng. Sci. 66 (2011) 5293–5300. https://doi.org/10.1016/j.ces.2011.07.028.
[21] Ö.E. Yıldırım, O.A. Basaran, Dynamics of formation and dripping of drops of deformation-rate-thinning and-thickening liquids from capillary tubes, J. Nonnewton. Fluid Mech. 136 (2006) 17–37. https://doi.org/doi:10.1016/j.jnnfm.2006.02.009.
[22] A. Lawal, R.A. Brown, The stability of an inclined pendent drop, J. Colloid Interface Sci. 89 (1982) 332–345. https://doi.org/10.1016/0021-9797(82)90185-0.
[23] N.C. Christov, K.D. Danov, D.K. Danova, P.A. Kralchevsky, The Drop Size in Membrane Emulsification Determined from the Balance of Capillary and Hydrodynamic Forces, Langmuir. 24 (2008) 1397–1410. https://doi.org/10.1021/la702306f.
[24] W.D. Harkins, F.E. Brown, The determination of surface tension (free surface energy), and the weight of falling drops - The surface tension of water and benzene by the capillary height method, J. Am. Chem. Soc. 41 (1919) 499–524. https://doi.org/10.1021/ja01461a003.
[25] P.M. Heertjes, L.H. de Nie, H.J. de Vries, Drop formation in liquid—liquid systems—I prediction of drop volumes at moderate speed of formation, Chem. Eng. Sci. 26 (1971) 441–449. https://doi.org/10.1016/0009-2509(71)83017-8.
[26] W. Wang, K.H. Ngan, J. Gong, P. Angeli, Observations on single drop formation from a capillary tube at low flow rates, Colloids Surf. A Physicochem. Eng. Asp. 334 (2009) 197–202. https://doi.org/10.1016/j.colsurfa.2008.10.011.
[27] E. Pitts, The Stability of a Drop Hanging from a Tube, IMA J. Appl. Math. 17 (1976) 387–397. https://doi.org/10.1093/imamat/17.3.387.
[28] D.H. Michael, P.G. Williams, The Equilibrium and Stability of Axisymmetric Pendent Drops, Proceedings of the Royal Society of London. Series A, Mathematical and

Journal Pre-proof

Physical Sciences. 351 (1976) 117–127. https://www.jstor.org/stable/79312 (accessed November 25, 2022).
[29] C.A. MacLeod, C.J. Radke, A Growing Drop Technique for Measuring Dynamic Interfacial Tension, J. Colloid Interface Sci. 160 (1993) 435–448. https://doi.org/10.1006/jcis.1993.1415.
[30] X. Zhang, M.T. Harris, O.A. Basaran, Measurement of Dynamic Surface Tension by a Growing Drop Technique, J. Colloid Interface Sci. 168 (1994) 47–60. https://doi.org/10.1006/jcis.1994.1392.
[31] A. Passerone, L. Liggieri, N. Rando, F. Ravera, E. Ricci, A new experimental method for the measurement of the interfacial tension between immiscible fluids at zero bond number, J. Colloid Interface Sci. 146 (1991) 152–162. https://doi.org/10.1016/0021-9797(91)90012-W.
[32] G.M. Walker, D.J. Beebe, A passive pumping method for microfluidic devices, Lab Chip. 2 (2002) 131–134. https://doi.org/10.1039/B204381E.
[33] E. Berthier, D.J. Beebe, Flow rate analysis of a surface tension driven passive micropump, Lab Chip. 7 (2007) 1475–1478. https://doi.org/10.1039/b707637a.
[34] A. Cobo, R. Sheybani, E. Meng, MEMS: Enabled Drug Delivery Systems, Adv Healthc Mater. 4 (2015) 969–982. https://doi.org/10.1002/adhm.201400772.
[35] E. Tronel-Peyroz, J.M. Douillard, L. Tenebre, R. Bennes, M. Privat, Associated complex formation in the liquid-vapor interface: the water-ethanol and water-tert-butyl alcohol systems, Langmuir. 3 (1987) 1027–1034. https://doi.org/10.1021/la00078a026.
[36] N.B. Vargaftik, B.N. Volkov, L.D. Voljak, International Tables of the Surface Tension of Water, J. Phys. Chem. Ref. Data. 12 (1983) 817–820. https://doi.org/10.1063/1.555688.
[37] M.L. Huber, R.A. Perkins, A. Laesecke, D.G. Friend, J.V. Sengers, M.J. Assael, I.N. Metaxa, E. Vogel, R. Mareš, K. Miyagawa, New International Formulation for the Viscosity of H2O, J. Phys. Chem. Ref. Data. 38 (2009) 101–125. https://doi.org/10.1063/1.3088050.
[38] P.K. Kipkemboi, A.J. Easteal, Densities and viscosities of binary aqueous mixtures of nonelectrolytes: tert-Butyl alcohol and tert-butylamine, Can. J. Chem. 72 (1994) 1937–1945. https://doi.org/10.1139/v94-247.
[39] O.I. del Rio, A.W. Neumann, Axisymmetric drop shape analysis: Computational methods for the measurement of interfacial properties from the shape and dimensions of pendant and sessile drops, J. Colloid Interface Sci. 196 (1997) 136–147. https://doi.org/doi.org/10.1006/jcis.1997.5214.
[40] J.L. Lando, H.T. Oakley, Tabulated correction factors for the drop-weight-volume determination of surface and interfacial tensions, J. Colloid Interface Sci. 25 (1967) 526–530. https://doi.org/10.1016/0021-9797(67)90064-1.
[41] T. Kaully, A. Siegmann, D. Shacham, A. Marmur, The effect of viscosity on surface tension measurements by the drop weight method, J. Appl. Polym. Sci. 106 (2007) 1842–1846. https://doi.org/10.1002/app.24567.

Journal Pre-proof

Highlights:

- Parametric growing drop model and mean flow rate of the drip at constant pressure
- Simplified Laplace-Young equation extended to non spherical pendant droplets
- Measurement of liquid surface tension by dripping with a camera and a capillary tip
- Dispense tips for drop injection in the middle-ear cavity and drug delivery systems
- Spherical drop shape modeling by video observations applied to elongated droplets

Journal Pre-proof

Author statement:

Thierry Thami carried out the experiment, wrote the manuscript and prepared the figures. Christian Fretigny and Emilie Verneuil wrote the manuscript, prepared the figures and performed physical model.

Journal Pre-proof

Journal Pre-proof

Declaration of interests

☒ The authors declare that they have no known competing financial interests or personal relationships that could have appeared to influence the work reported in this paper.

☐The authors declare the following financial interests/personal relationships which may be considered as potential competing interests:

Journal Pre-proof